CHAPTER 3

FIELD AND FORCE CALCULATIONS

3.1 2-Dimensional Field Calculations

Because the overall geometry of the solenoid inserted in the existing toroid magnet system of the DØ detector is rather complicated, field calculations were done in three steps. The first step was to model the solenoid surrounded by the thick steel of the toroidal magnet system but with the latter unexcited. This calculation provides a field map sufficiently accurate to enable the evaluation of potential interaction between the solenoid and the various existing detector elements in the fringe field of the solenoid.

In this first calculation the system was assumed axisymmetric and field values were calculated with the 2 dimensional finite element analysis program ANSYS [1]. The result is shown in Figure 2.1. In this calculation, the solenoid is excited, but not the toroids. The magnetic field of the solenoid on the surface of the toroidal steel is up to 330 Gauss.

To model the solenoidal field more accurately near and inside the coil a much more detailed local calculation was required. Using the solution from step one, boundary conditions for a smaller region containing the coil were obtained and a second calculation on a much finer mesh (2 cm) was made of the region near the solenoid coil. The restricted boundary was remote enough from the solenoid so as not to significantly affect the calculation but the boundary conditions were necessary to constrain the new solution. The field values from this solution are particularly valuable for studying the homogeneity of the field in the bore of the magnet, especially as it relates to tracking issues such as pattern recognition and charged particle momentum resolution $\Delta p_\perp/p_\perp$.

In a final step, a very fine mesh (5 mm) was used for a solution of the field near the coil. This solution was useful in studying the field in regions within the coils.

3.2 Detailed Field Calculations Near the Solenoid

The total magnetic field distribution and axial magnetic field distribution inside the solenoidal volume are shown in Figures 3.1 and 3.2, respectively. The field values in these figures are normalized to the central field value of the solenoid (2 Tesla), and plotted as a percentage of this value. The two field peaks near the end of the winding are due to the increased current density caused by the change of conductor width. The locations where the change of conductor widths and missing turns occur are marked with arrows. A detailed study shows that the maximum total magnetic field is 2.174 T at the outside edge of the inner layer

conductor. Select values of the pseudorapidity variable $\eta = -log(tan\theta/2)$ which is derived from the scattering angle θ are also plotted in these figures.

A 3-dimensional isometric representation of the axial field distribution inside the solenoidal region is shown in Figure 3.3. From this figure it is clearly seen that the axial field is reasonably constant over the majority of the solenoidal volume. Figure 3.4 shows the reverse side of this plot illustrating the negative return flux distribution.

3.3 Integrated Field Uniformity

To quantitatively describe the inhomogeneity of the magnetic field inside the solenoidal volume, a calculation that defines the inhomogeneity of the field as a function of scattering angle from the center of the magnet is made. This calculation takes the form of an integral over the path along an angle from the center to the coil or the coil end plane, depending on the azimuthal scattering angle θ:

$$Inhomogeneity \;=\; \frac{1}{B_o L(\theta)} \int_o^p (B_z - B_o) dl$$

where B_z is the axial magnetic field along the path $L(\theta)$, p the endpoint of the path, θ the scattering angle, and B_o the field at the center of the solenoid (2 Tesla).

The result of this calculation as a function of the angle θ is shown in Figure 3.5. The integrated field error is less than 3% in the range from 28 degrees to 152 degrees in scattering angle. There are slight fluctuations caused by the missing turns where the conductor transition joints are located, but these are unimportant.

3.4 3-Dimensional Field Calculations

A three dimensional field calculation of the entire detector was performed by the TOSCA [2] program using a 10 cm grid. First the field of the existing toroid system was calculated without the the solenoid in order to compare the results to the measured values from the toroids. When the B-H curves used with the TOSCA program were modified to give consistent data with the measured results, the solenoidal coils were added and the results were compared to the two dimensional ANSYS calculation. The flux distribution in the toroid steel is not affected greatly by the fringing field of the solenoid, partly because the toroid steel is already strongly saturated by the toroid coils. There is however a small effect noticeable along the toroid steel surface caused by the solenoid.

3.5 Decentering Forces

Three approaches have been taken to estimate the forces between the coil and the toroid steel; one is totally analytic, one is mixed (i.e. partly analytic and partly discrete) and the third uses ANSYS to estimate the axial forces. Because the coil is nominally centered in the yokes of the EF and CF toroids the net force on the coil is nominally zero; the calculations in all cases predict that the radial and the axial forces generated by small displacements are decentering. Because the coil is quite far from the steel both radially and axially the forces for reasonable displacements are predicted to be modest. The corresponding minimum stiffness required of the cold-mass suspension system is likewise modest.

3.5.1 Analytic Approach: "Ideal Dipole"

For the fully analytic approach the solenoid is modeled as an ideal dipole and the toroid yokes as semi-infinite sheets of infinitely permeable iron. The dipole moment of the ideal dipole is just the total solenoidal current times the cross-sectional area of the coil, and the forces are generated by this dipole interacting with image dipoles mirrored in the iron.

The net axial force on an ideal dipole centered between semi-infinite regions of infinitely permeable steel separated from one another a distance 2D is of course zero, but if the dipole is shifted an amount Δ off center axially it can be shown that a decentering force created by the image dipoles in the EF steel acts on the dipole:

$$\left.\frac{F}{\Delta}\right|_{restor} = \frac{\mu_o 3M^2}{4\pi D^5}.$$

Hence, for the solenoid in the EF steel, the axial decentering force, in the direction of Δ is:

$$\begin{aligned}\left.\frac{F}{\Delta}\right|_{restor} &= \frac{(4\pi\times 10^{-7})\times 3\times(6.08\times 10^6)^2}{4\pi\times(1.1^5)}[\frac{N}{m}] \\ &= 6.72\times 10^3[\frac{N}{m}],\end{aligned}$$

inserting the values pertaining to the DØ solenoid. The cold-mass suspension system must have axial stiffness greater than this to support the coil stably. For an axial displacement of e.g. 2.5 cm, the decentering force in the direction of the displacement is $F = 6.72\times 10^3\times 0.025\,N = 168\,N$.

For the solenoid in the CF steel, it can be shown that the radial decentering force due to image dipoles mirrored in the steel, in the direction of the displacement Δ, is:

$$\left.\frac{F}{\Delta}\right|_{restor} = \frac{\mu_o M^2}{4\pi D^5}.$$

Again inserting the values pertaining to the DØ solenoid,

$$\left.\frac{F}{\Delta}\right|_{radial} = \frac{(4\pi \times 10^{-7}) \times (6.08 \times 10^6)^2}{4\pi \times (3.2^2)} [\frac{N}{m}]$$
$$= 1.10 \times 10^4 [\frac{N}{m}].$$

For a radial displacement of e.g. 2.5 cm the decentering force in the direction of the displacement is $F = 1.10 \times 10^4 \times 0.025\, N = 278\, N$.

3.5.2 Mixed Approach: "Image Solenoid"

For the "image solenoid" analytic approach the primary solenoid is subdivided into many current loops with each loop subdivided into many small phi-segmented current elements, and the forces generated by solenoids mirrored in the CF and EF steel yokes. The fields of the image solenoids are calculated by subdividing them in the same fashion as is done for the primary solenoid, and using a subroutine which evaluates elliptical integrals to provide the fields at each segment of current of the subdivided β coil. The solenoids are subdivided into 20 axial and 10 radial current loops, and each loop divided into 40 phi-segments. This level of discretization is sufficiently accurate to predict the central fields to 1/4 %.

The image field $\vec{B}(r,z)$ at a current element at (r,z) of the primary solenoid is a sum of $\vec{B}^i + \vec{B}^r$, where, explicitly, $\vec{B}^r(r,z) = \mathbf{B}$(r,z-2(D-$\Delta$)), and $\vec{B}^i(r,z) = \mathbf{B}$(r,z+2(D + Δ)). The force on the current element is just the vector product of this field and the current in the element times its length; the total force on the solenoid is then a sum over all the current elements in the coil.

When the parameter Δ was set to zero the net calculated forces in the transverse and axial directions were less than $10^{-2} N$, indicating that the discretizations were adequate.

For $\Delta = 10$ cm. we obtain

$$F_x \approx F_y \approx 0.0\, N$$
$$F_z = +0.625\pi 10^3\, N.$$

Assuming linearity for small displacements Δ, the axial decentering force in the direction of Δ is predicted to be:

$$\left.\frac{F}{\Delta}\right|_{axial} = 6.25 \times 10^3 [\frac{N}{m}].$$

For an axial displacement of e.g. 2.5 cm, in the direction of the displacement, $F = 6.25 \times 10^3 \times 0.025\, N = 156\, N$.

For the radial case, the solenoid is located between two semi-infinite sheets of steel above and below it, and the forces on the solenoid are calculated as described above. The results for $\Delta = 10$ cm. are:

$$\begin{aligned} F_x &\approx F_z \approx 0.0\,N \\ F_y &= +0.801 \times 10^3\,N. \end{aligned}$$

Again assuming linearity for small displacements,

$$\left.\frac{F}{\Delta}\right|_{radial} = 8.01 \times 10^3 [\frac{N}{m}],$$

in the direction of Δ. For a radial displacement of e.g. 2.5 cm, in the direction of the displacement, $F = 8.01 \times 10^3 \times 0.025\,N = 200\,N$.

These results are quite comparable to those obtained from the "ideal dipole" approach, although since the ideal solenoid approach calculates the image fields directly without using any "dipole approximations", it might be expected to give a more realistic result.

3.5.3 Fully Discrete Approach: ANSYS

The axial decentering force has also been calculated using ANSYS by making a 2-dimensional axisymmetric model of the entire solenoid and toroid systems. In this model the solenoid itself is shifted by 2.5 cm on the z axis and the resultant force computed by summing all the axial forces on the solenoid. The total axial decentering force is 1731 N (0.176 metric tons, or 389 lb) corresponding to 6.9 x 10^4 N/m.

The estimated forces for the solenoid are in general much smaller than those for magnets which involve steel in the near vicinity, e.g. ZEUS, where the solenoid is placed asymmetrically and the axial decentering force is 5 Tons, or for CDF where the axial decentering force is 1.8 Tons/cm.

3.6 Stress Calculations by ANSYS

Because the toroid steel is remote from the solenoid there is a substantial radial field component along the coil which increases toward the ends of the magnet. This radial field produces significant axial compressive force in the coil which increases with increasing distance from the coil center. ANSYS was used to calculate the corresponding stress and that from the hoop loads as well.

Provided with the appropriate geometry in a predefined region ANSYS first calculates the magnetic field, and then the Lorentz forces on the coil, for the problem specified. Then ANSYS evaluates the stresses on the coil and support cylinder elements specified in the region. For these stress calculations the outer air boundary was constrained to a fixed

potential determined from a full scale 2-dimensional axisymmetric model of the detector including the toroid magnets. The mesh for the coil and support cylinder in this full scale model were not fine enough to determine peak stresses on the coil. Therefore a much finer mesh and model were created around the solenoid for stress analysis and the results of this smaller model are used in this analysis.

A number of assumptions about the solenoid model are implicit in this analysis. The model is 2-dimensional and is assumed to be axisymmetric, and the middle point of the solenoid and support cylinder (the left boundary of the model) is constrained to a movement of 0.0 m in the Z direction. The bond between the coil and support cylinder is assumed inseparable, and the modulus of elasticity used for the solenoid is $6.86 \times 10^{10} N/m^2$ for the combined structure of the coil and support cylinder. This value comes from the CDF R&D test coil [3]. The results of the ANSYS calculations are shown in Figure 3.7 and 3.8 and the extrema of these curves are tabulated in Table 3.1. Note that although the origin of the loads on the coil are the conductors themselves, the model incorporates the support cylinder together with the coil as a monolithic structure.

The hoop stresses generated in the coil are equilibrated by strain in the support cylinder and coil; the highest hoop stress in the conductor is 20.8 MPa (Table 3.1). From Figure 3.8 it is seen that the peak axial and hoop stresses in the coil are at nearly the same Z location. Thus we combine them using the Von Mises criterion (they are the principle stresses) to obtain an effective total stress of 27.9 MPa. This is well within the limit set for the pure aluminum, taken to be 44.15 MPa (6400 psi), as shown in Figure 3.6.

3.7 Analytic Hoop Stress Analysis

When cooled to 5.0 K, the length of the outer support cylinder is reduced by $\Delta L = L \times 4.3 \times 10^{-3} = 11$ mm due to thermal contraction effects. Because the cylinder is axially constrained only at the current lead end (see Chapter 4), most of this motion appears at the other end of the coil and no new stresses on the coil result. Similarly, the radius of the support cylinder is reduced by $\Delta R = R \times 4.3 \times 10^{-3} = 2.8$ mm during cooldown, and the radial support system is designed so that small added stresses on the coil result from this motion.

During cooldown the support cylinder is cooler than the conductor and this will ensure that the support cylinder always remains compressively loaded onto the coil windings. Because the temperatures experienced in the support cylinder and the coil always remain well below 100K during a quench the support cylinder will not be subject to unwanted differential thermal expansion from the coil. Warm up of the magnet will be achieved without generating excessive temperature difference between the coil and the support cylinder.

When the magnet is excited, the conductor winding pushes the support cylinder outward

with the magnetic pressure **P**

$$P = \frac{B^2}{2\mu_o} N/m^2 = 1.59 MPa$$

The increase in radius **R** of the support cylinder due to such an internal pressure is given by

$$\epsilon = \frac{\Delta R}{R} = \frac{\sigma}{E} = \frac{1}{E}\frac{PR}{t}$$

where **E** is the Young's modulus of aluminum, $7.6 \times 10^{10}\, Pa$ $(1.1 \times 10^7 psi)$ at 4.2 **K**. And t is the summed radial thickness of the coil and the support cylinder. With t = 1.5 cm and **R** = 52 cm,

$$\begin{aligned} \epsilon &= 2.5 \times 10^{-4} \\ \Delta R &= 0.13mm \\ \sigma &= 18.7 MPa \end{aligned}$$

The coil winding and support cylinder will expand approximately 0.26 mm in diameter due to the magnetic pressure.

3.8 Displacement of Solenoid and Support Cylinder

ANSYS also calculates the displacement of the support cylinder and coil due to hoop and axial stresses. An exaggerated picture of the displaced and undisplaced superconductors and support cylinder is shown in Figure 3.9. The amount of displacement in the support cylinder and conductor are graphed in Figures 3.10 and 3.11. The displacement results obtained from ANSYS are also summarized in Table 3.1

References

[1] Swanson Analysis Systems, Inc., PO Box 65, Houston, Pennsylvania 15342

[2] Vector Fields Inc., 1700 North Farnsworth Ave, Aurora, IL, (tel)708-851-1734 and Vector Fields Ltd., 24 Bankside, Kidlington, Oxford OX5 1JE, England, (tel)0865 - 370151

[3] R. W. Fast, *et.al.* "Design Report for an Indirectly Cooled 3-m Diameter Superconducting Solenoid for the Fermilab Collider Detector Facility", Fermilab Internal Report TM-1135, Oct. 1, 1982.

TABLE 3.1: Stress and Displacement of the Solenoid			
Parameter	Units	Maximum	Minimum
Coil Hoop Stress	MPa	20.80	11.09
Coil Axial Stress	MPa	10.99	2.26
Coil Total Displacement	mm	0.28	0.18
Support Cylinder Hoop Stress	MPa	23.25	12.36
Support Cylinder Axial Stress	MPa	10.79	0.00
Support Cylinder Total Displacement	mm	0.285	0.18
Axial Decentering	N/m	$6.9x10^4$	
Radial Decentering	N/m	$1.1x10^4$	

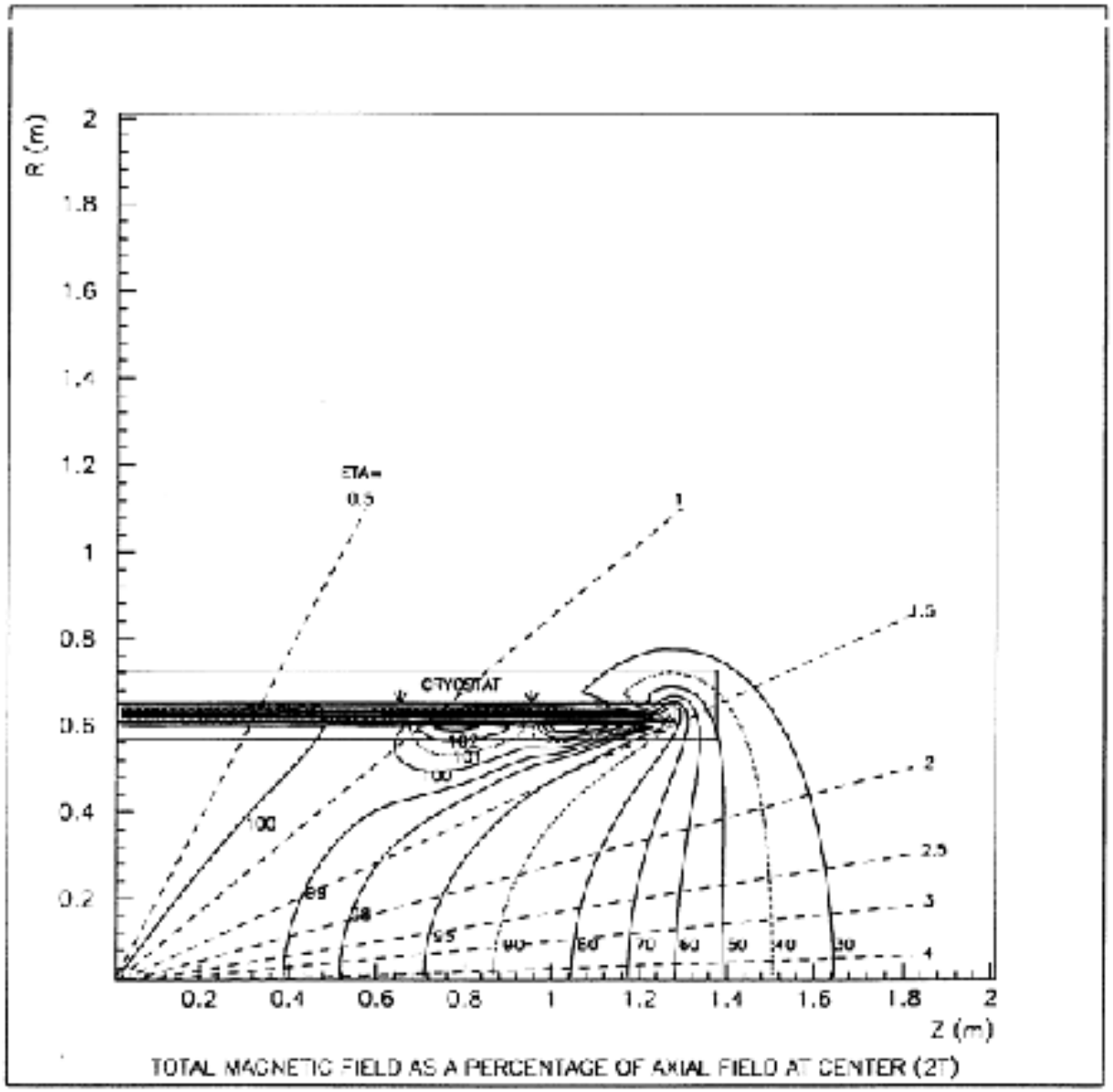
R (m)
Z (m)
ETA=
0.5
1
1.5
2
2.5
3
4
CRYOSTAT
TOTAL MAGNETIC FIELD AS A PERCENTAGE OF AXIAL FIELD AT CENTER (2T)

Figure 3.1

R (m)
Z (m)
ETA=
0.5
CRYOSTAT
TMN
BZ AS A PERCENTAGE OF AXIAL FIELD AT CENTER (2T)

Figure 3.2

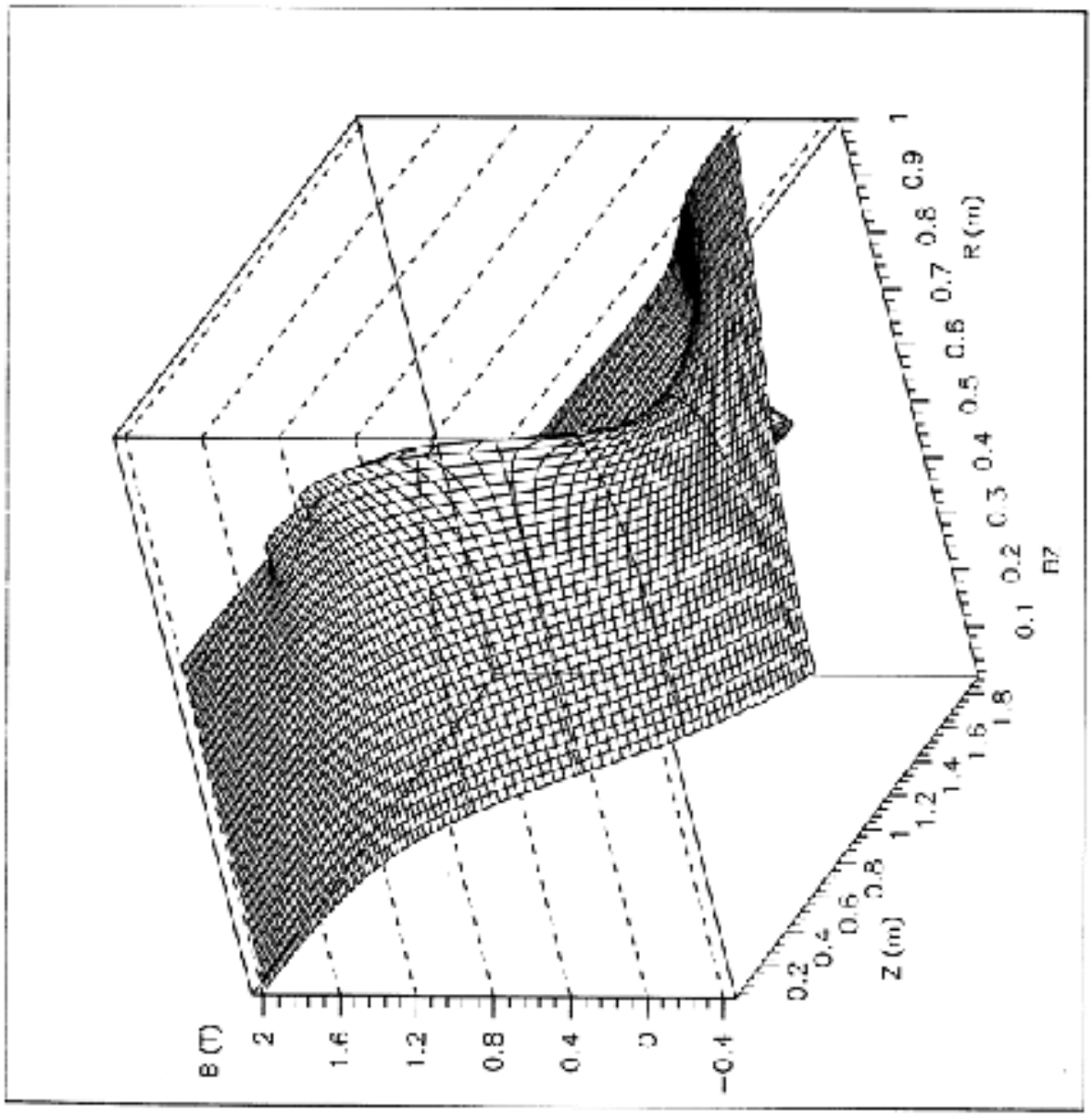
B (T)
2
1.6
1.2
0.8
0.4
0
−0.4
Z (m)
0.2
0.4
0.6
0.8
1
1.2
1.4
1.6
1.8
R (m)
0.1
0.2
0.3
0.4
0.5
0.6
0.7
0.8
0.9
1

Figure 3.3

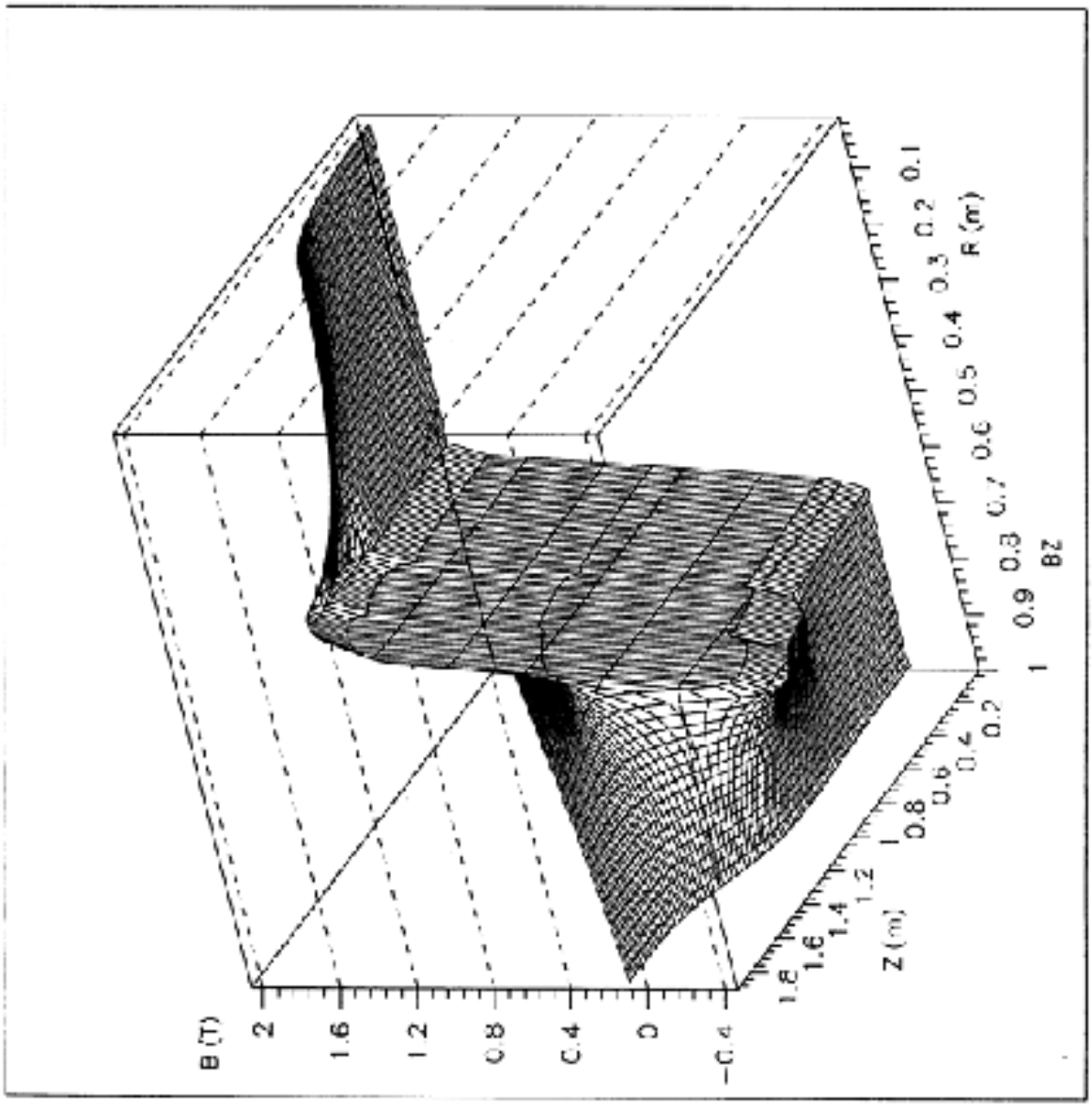
B (T)
2
1.6
1.2
0.8
0.4
0
−0.4
Z (m)
1.8
1.6
1.4
1.2
1
0.8
0.6
0.4
0.2
R (m)
1
0.9
0.8
0.7
0.6
0.5
0.4
0.3
0.2
0.1

Figure 3.4

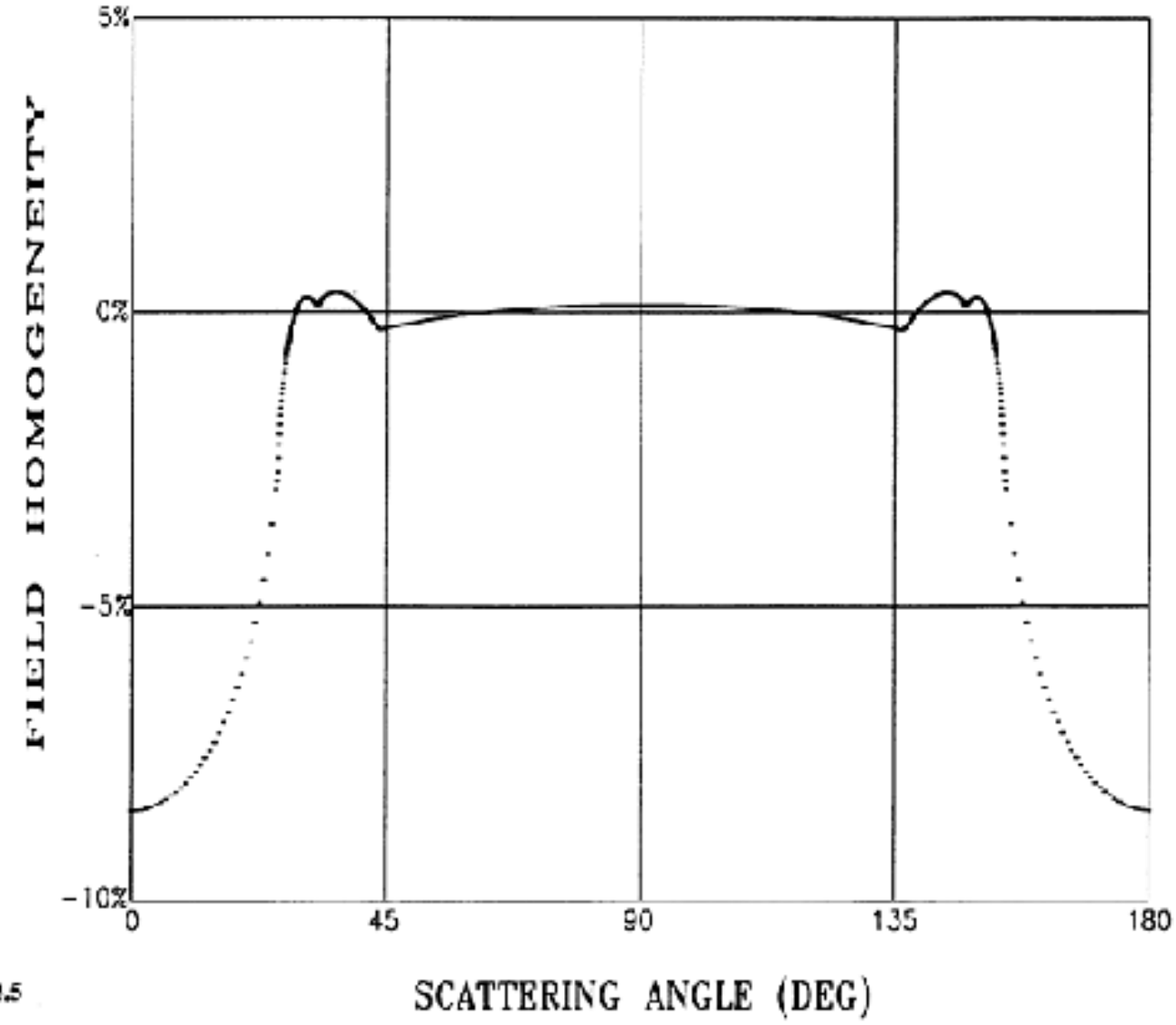
5%
0%
-5%
-10%
FIELD HOMOGENEITY
0
45
90
135
180
SCATTERING ANGLE (DEG)

Figure 3.5

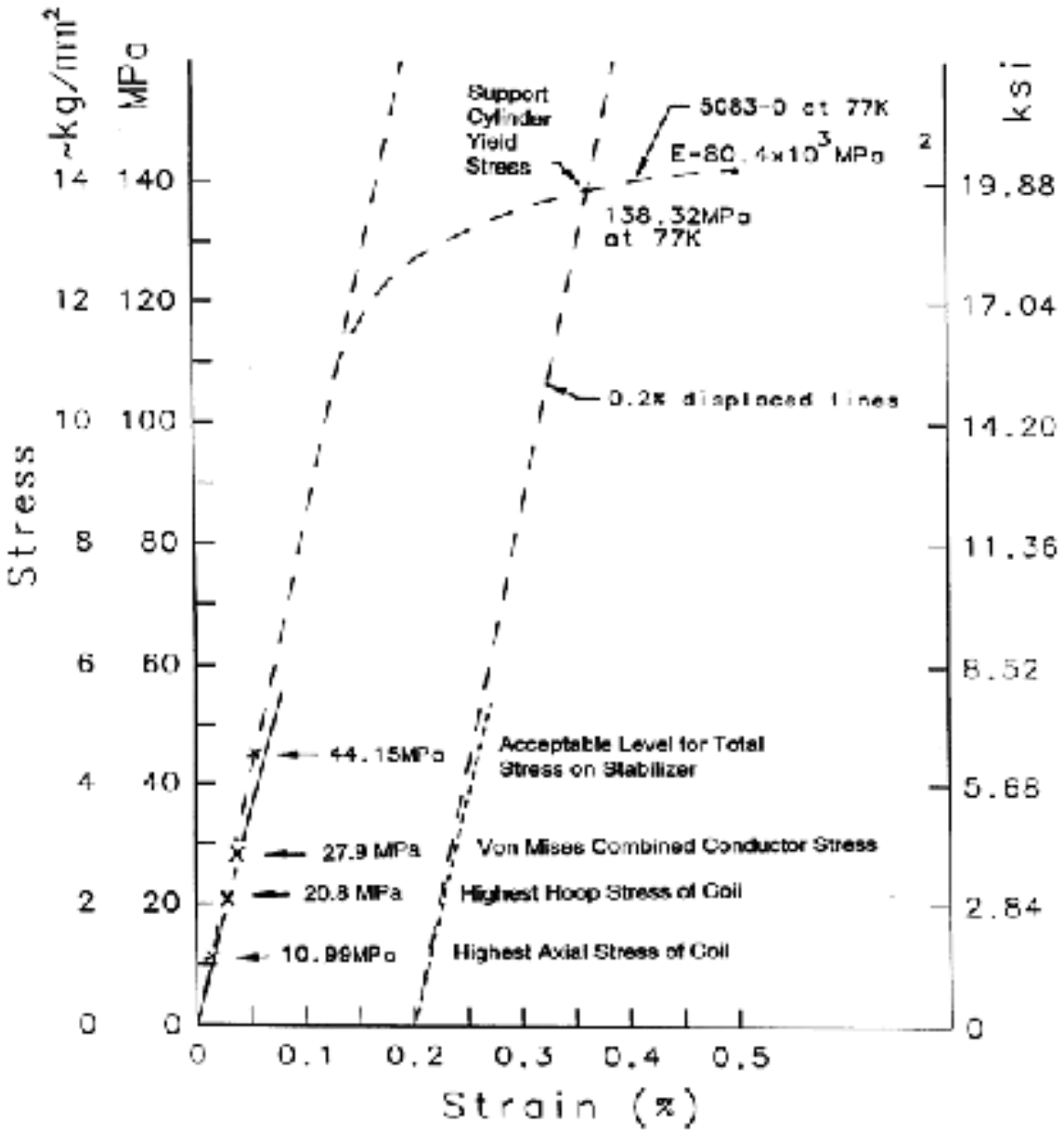

Fig 3.5 Estimated stress-strain curve

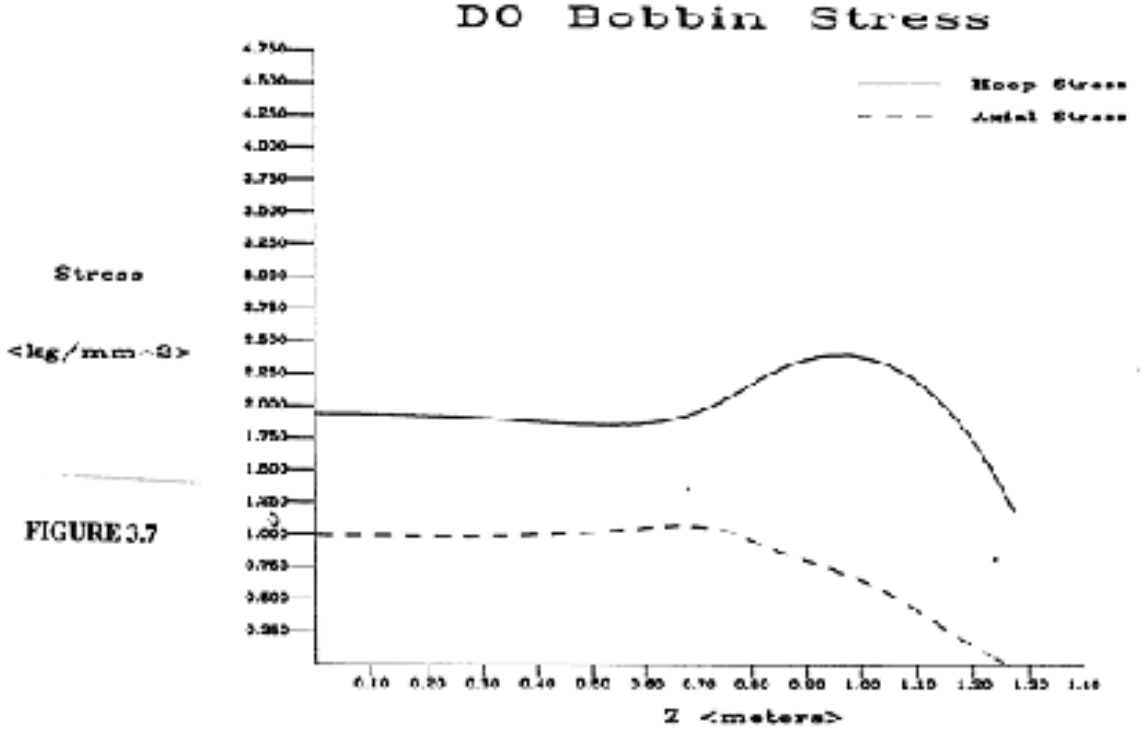

FIGURE 3.7

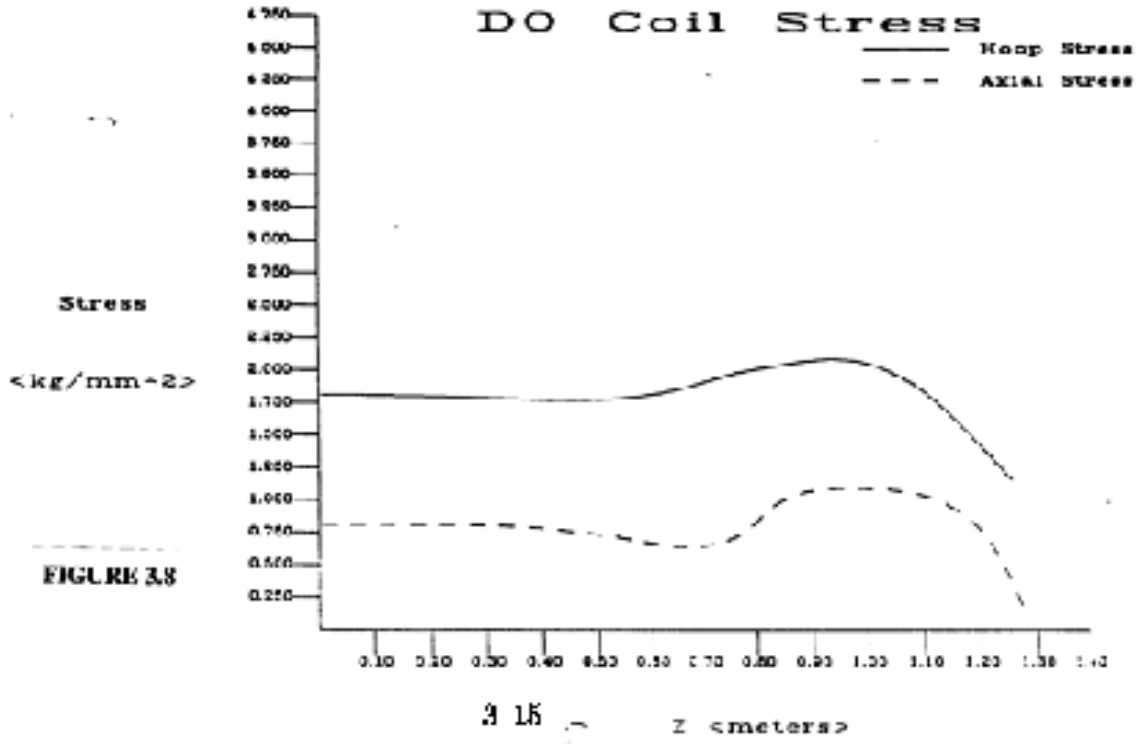

FIGURE 3.8

figure 3.9 : Coil and Bobbin Displacement

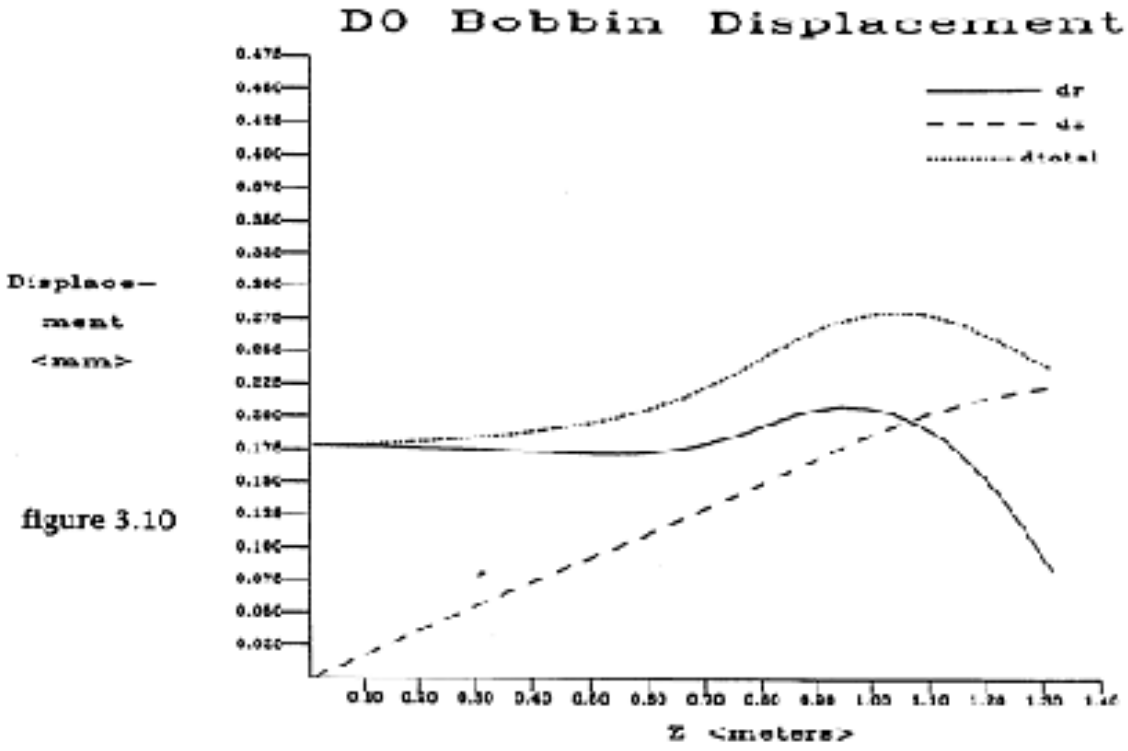

figure 3.10

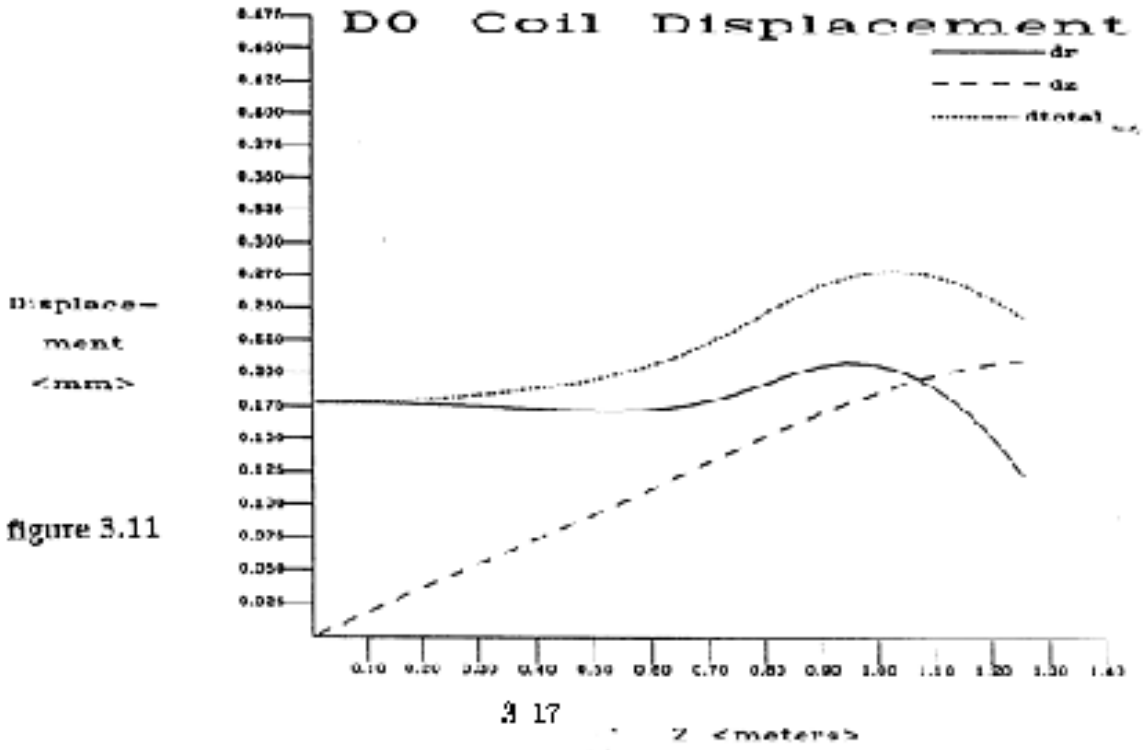

figure 3.11